

# A new apparatus for measuring mechanical properties at moderate confining pressures in a neutron beamline

Stephen J. Covey-Crump,<sup>a\*</sup> Robert F. Holloway,<sup>a</sup> Paul F. Schofield<sup>b</sup> and Mark R. Daymond<sup>c,d</sup>

<sup>a</sup>School of Earth, Atmospheric and Environmental Sciences, University of Manchester, Williamson Building, Oxford Road, Manchester M13 9PL, UK, <sup>b</sup>Department of Mineralogy, Natural History Museum, Cromwell Road, London SW7 5BD, UK, <sup>c</sup>Department of Mechanical and Materials Engineering, Queen's University at Kingston, Kingston, Ontario K7L 3N6, Canada, and <sup>d</sup>ISIS Neutron Facility, Rutherford Appleton Laboratory, Chilton, Didcot, Oxfordshire OX11 0QX, UK. Correspondence e-mail: s.covey-crump@manchester.ac.uk

A simple pressure vessel suitable for use at room temperature has been developed which allows neutron diffraction data to be collected from cylindrical samples of up to 10 mm diameter, at confining pressures of up to 160 MPa, whilst they are also being deformed in compression by the application of a uniaxially symmetric load. The vessel has been commissioned on the ENGIN-X beamline at the ISIS neutron facility (Rutherford Appleton Laboratory, Chilton, UK). The commissioning results show that neutron diffraction data of quality equivalent to that obtained using an identical experiment geometry at room pressure can be acquired using the pressure vessel with only about a factor of two increase in count times.

© 2006 International Union of Crystallography  
Printed in Great Britain – all rights reserved

## 1. Introduction

In recent years a number of neutron facilities have developed the capacity to perform deformation experiments within the neutron beamline on polycrystalline metallurgical and geological samples of the order of 50 to 1500 mm<sup>3</sup> in size (*e.g.* Daymond *et al.*, 1997; Carter & Bourke, 2000; Covey-Crump *et al.*, 2001). By collecting neutron diffraction data at different applied loads, the load dependence of the lattice spacings can be determined, thereby providing important insight, not easily obtained by other means, as to how the deformation is accommodated within the sample at the grain scale. At the same time, the development of electron back-scatter diffraction techniques (Adams *et al.*, 1993; Prior *et al.*, 1999) has made it possible to obtain extremely rapidly a wealth of grain-scale microstructural information from previously deformed samples. Together, these two developments allow those theoretical analyses that seek to specify the mechanical properties of polycrystalline materials from the single-crystal properties of their constituents to be much more rigorously tested than was possible before when experiments provided only whole-sample mechanical properties and the requisite grain-scale microstructural analyses were extremely time consuming.

The deformation experiments that have been performed so far in neutron beamlines on large samples have all been conducted either at room pressure and temperature or at room pressure and elevated temperatures. However, confining pressure is often an important variable, notably in systems

where the deformation leads to a mechanically induced phase transformation which involves a volume change. In addition, confining pressure helps to suppress brittle deformation and so by conducting experiments at elevated confining pressures, elastic and plastic flow properties can be examined over a greater range of load and temperature than would otherwise be the case. This is particularly important when investigating the mechanical behaviour of geological materials because almost all of the volumetrically significant minerals have a strong tendency for brittle failure at room pressure.

There has been some success in recent years in modifying multi-anvil and Paris–Edinburgh type apparatus to allow deformation experiments at very high confining pressure (>1000 MPa) to be performed at synchrotron X-ray sources and neutron facilities, respectively (Durham *et al.*, 2002; Dobson *et al.*, 2005). Such experiments necessarily involve the use of very small samples to achieve the requisite pressures, and consequently the quality of the mechanical data is to some extent compromised by the effects of stress heterogeneities arising within the specimen as a result of the geometry of the sample assembly. At more modest confining pressures (10–300 MPa) this difficulty can be avoided by using large samples. However, this, in turn, requires the use of a thick-walled pressure vessel. The principal difficulty which then follows is that the neutrons must pass through the pressure-vessel wall as well as the sample, thereby reducing the quality of the diffraction data and increasing the count times required to obtain usable results. To counter this problem, in isostatic experiments performed in this pressure range, high-strength

aluminium alloys (which take advantage of the relatively high transparency of aluminium to neutrons) have been successfully used as the pressure-vessel material (*e.g.* Smith *et al.*, 1966; Lechner, 1966; Paureau & Vettier, 1975).

In this paper we describe a new apparatus in which the pressure vessel is made from aluminium alloy, which allows room-temperature axial-compression experiments to be performed on large cylindrical samples at confining pressures of up to 160 MPa in a neutron beamline. In common with other apparatus used for large-sample deformation experiments at elevated confining pressures (*e.g.* Paterson, 1990), a key element of the design lies in the internal force gauge which monitors the differential load experienced by the sample directly, so that no corrections for that part of the total applied load (as seen by an external load cell) taken up in overcoming friction at the moving piston seals needs to be made. The apparatus has been successfully commissioned on the ENGIN-X beamline (Johnson & Daymond, 2002; Dann *et al.*, 2004) at the ISIS neutron facility (Rutherford Appleton

Laboratory, Chilton, UK) in a set of experiments designed to investigate the pressure dependence of the austenite to martensite transformation of NiTi under an applied uniaxial stress. The commissioning experiments show that there is considerable scope for modifications to the dimensions of the design to allow the use of larger samples and/or higher confining pressures. Consequently, so that others can evaluate independently what dimensional modifications are feasible, the design considerations bearing most directly on this matter are described in more detail.

## 2. Room-pressure experimental setup

In order to provide some context for a discussion of the design issues, the geometry of the experimental setup for axial compression experiments at room pressure and temperature on the ENGIN-X beamline at ISIS is briefly described. A more detailed account is given elsewhere (Schofield *et al.*, 2003).

For axial compression experiments, the samples are right circular cylindrical cores, 10 mm in diameter by about 25 mm long. It is important if the experimental measurements are to be reproducible on different samples that the sample diameter be at least ten times the mean grain size, but also that it should not be so large that the loads required to achieve the desired applied stresses become prohibitive. It is also important in compression experiments that the sample length be about 2.0 to 2.5 times the diameter because at smaller lengths the stress heterogeneities generated by the frictional forces at the piston/sample interfaces compromise the interpretation of the mechanical data (Birch *et al.*, 1976), whereas at larger lengths sample buckling becomes an issue (Cropper & Pask, 1969).

The samples are loaded in a 50 kN hydraulic Instron load frame positioned such that the loading axis is horizontal and at 45° to the incident beam (Fig. 1; see also Daymond & Priesmeyer, 2002). The neutron data are collected as time-of-flight powder diffraction data in two fixed-angle detector banks at  $\pm 90^\circ$  to the incident beam. On ENGIN-X, the incident neutrons are polychromatic and so a complete diffraction pattern is collected in each detector. With this experiment geometry the detector bank to the right of the sample (as pictured in Fig. 1) records neutrons diffracted from lattice planes with scattering vectors parallel to the loading direction, and hence monitors lattice strains in that direction, while the other detector records neutrons diffracted from lattice planes with scattering vectors normal to the loading direction, and hence monitors lattice strains in this second direction.

The normal experimental procedure is to apply a small load to the sample and to hold it at that load while the neutron diffraction data are collected. Once a diffraction pattern of sufficient quality has been obtained, the sample is taken to a new load and held there while a further set of neutron data are collected. This process is repeated until neutron diffraction patterns from a number of loads have been obtained. Throughout the experiment, the applied load and crosshead position are monitored. In addition, the bulk strain parallel to

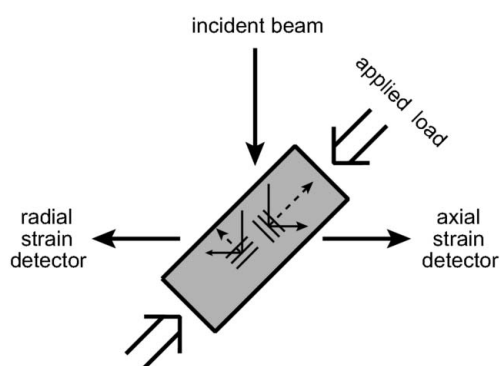
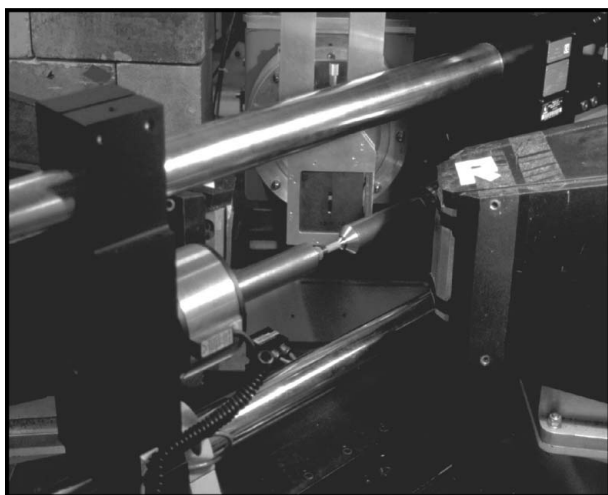


**Figure 1**

Geometry of the experimental setup. Top: photograph of the specimen assembly on the ENGIN beamline (the forerunner to ENGIN-X) at ISIS. The sample is held within the Instron load frame at 45° to the incident neutron beam. The neutron detectors are at  $\pm 90^\circ$  to the incident beam. Bottom: a schematic plan view of the experimental arrangement. In this geometry the detector to the right of the sample detects neutrons with scattering vectors parallel to the loading direction, while the detector to the left of the sample detects neutrons with scattering vectors normal to the loading direction.

**Table 1**

Approximate attenuation lengths ( $l = 1/e$ ) for thermal neutrons (25 meV) for elements commonly found in thick-walled pressure-vessel materials.

The data come from the tabulation of Hutchings & Windsor (1987): the atomic weights ( $A$ ) and material densities ( $\rho$ ) are as tabulated by them, and the microscopic coherent, incoherent and absorption cross sections ( $\sigma_c$ ,  $\sigma_i$ ,  $\sigma_a$ , respectively) were calculated using these  $A$  and  $\rho$  from their tabulated macroscopic coherent, incoherent and absorption cross sections ( $\Sigma_c$ ,  $\Sigma_i$ ,  $\Sigma_a$ , respectively).  $\Sigma_{total} = \Sigma_c + \Sigma_i + \Sigma_a$  and  $l = 1/\Sigma_{total}$ .

	$A$ (g mol <sup>-1</sup> )	$\rho$ (g cm <sup>-3</sup> )	$\sigma_c$ (barn)	$\sigma_i$ (barn)	$\sigma_a$ (barn)	$\Sigma_{total}$ (cm <sup>-1</sup> )	$l$ (cm)
Al	26.98	2.698	1.496	0.008	0.231	0.1045	9.57
C	12.01	2.266	5.557	0.001	0.004	0.6319	1.58
Co	58.95	8.800	0.785	4.802	37.199	3.8463	0.26
Cr	52.01	7.194	1.662	1.831	3.071	0.5467	1.83
Cu	63.54	8.933	7.489	0.520	3.782	0.9982	1.00
Fe	55.85	7.873	11.443	0.390	2.561	1.2219	0.82
Mg	24.31	1.741	3.631	0.077	0.063	0.1626	6.15
Mn	54.94	7.473	1.749	0.400	13.307	1.2661	0.79
Mo	95.95	10.222	6.073	0.281	2.552	0.5713	1.75
Ni	58.71	8.907	13.338	5.202	4.492	2.1043	0.48
Si	28.09	2.329	2.165	0.016	0.170	0.1174	8.52
Ti	47.90	4.508	1.369	2.671	6.093	0.5743	1.74
V	50.95	6.090	0.018	5.189	5.082	0.7406	1.35
Zn	65.38	7.135	4.057	0.078	1.111	0.3447	2.90
Zr	91.22	6.507	6.446	0.161	0.184	0.2917	3.43

**Table 2**

Approximate attenuation lengths ( $l = 1/e$ ) for thermal neutrons (25 meV) of two widely used materials for thick-walled pressure vessels in experimental rock-deformation laboratories, and for the 7075 Al alloy used for the pressure vessel described in this paper.

The macroscopic coherent, incoherent and absorption cross sections were calculated using the data in Table 1 and the method of Hutchings & Windsor (1987); the alloy densities were determined assuming that atomic volumes are conserved.

Material†	$\rho$ (g cm <sup>-3</sup> )	$\Sigma_c$ (cm <sup>-1</sup> )	$\Sigma_i$ (cm <sup>-1</sup> )	$\Sigma_a$ (cm <sup>-1</sup> )	$\Sigma_{total}$ (cm <sup>-1</sup> )	$l$ (cm)
AISI H13 steel	7.587	0.8730	0.0418	0.2146	1.1294	0.89
Nimonic105	7.592	0.6104	0.3119	0.8200	1.7423	0.57
7075 Al alloy	2.792	0.0994	0.0010	0.0165	0.1169	8.56

† AISI H13 steel: 90.72% Fe, 5.2% Cr, 1.4% Mo, 1.0% Si, 0.9% V, 0.4% Mn, 0.38% C (weight %). Nimonic105: 51.6% Ni, 20.0% Co, 15.0% Cr, 5.0% Mo, 4.7% Al, 1.2% Ti, 0.8% Zr, 0.5% Fe, 0.5% Mn, 0.5% Si, 0.1% C, 0.1% Cu (weight %). 7075 Al alloy: 90.1% Al, 5.6% Zn, 2.5% Mg, 1.6% Cu, 0.2% Cr (weight %).

the loading direction is monitored using a capacitance extensometer or strain gauge attached to the sample.

### 3. Pressure-vessel design considerations

For the experiments at high confining pressure it is convenient to retain the geometry used for the room-pressure experiments. The use of a thick-walled cylindrical pressure vessel allows this. We wanted to avoid the design complexities associated with building a vessel containing windows made of a neutron-transparent material for the incident and diffracted neutron beams to pass through. Consequently, we needed to find a material for the pressure vessel which was relatively transparent to neutrons, but which also had the mechanical properties necessary to sustain the stresses caused by the

required confining pressures. For thick-walled pressure vessels designed for high-pressure experiments under isostatic conditions at room temperature or below, aluminium alloys have been found to satisfy these requirements.

As a basis for assessing the advantages of aluminium over other possible pressure-vessel materials, which is pertinent given its limited suitability for higher-temperature applications, approximate neutron attenuation lengths for a number of elements which are commonly found in materials used in thick-walled pressure vessels are shown in Table 1. From this table, on purely neutron-penetration considerations alone (but see Withers, 2004a,b, for other factors to consider) the advantages of aluminium are clear. The use of an aluminium alloy rather than a material such as vanadium that has negligible coherent elastic scattering (*i.e.* no diffraction peaks) is predicated on the ability to define a gauge or scattering volume within the pressure vessel itself, such that diffraction peaks are only obtained from the sample without contamination of peaks from the pressure vessel. In principle, the use of slits on the incident beam and radial collimators on the diffracted beam should allow this on the ENGIN-X beamline, although a small amount of contamination from aluminium scattering was seen for the gauge used (see §6).

The mechanical, physical and chemical properties of a wide range of aluminium alloys have been made freely accessible by the European Aluminium Association (<http://aluminium.matter.org.uk/aluselect/default.asp>). Of these alloys, the 7000 series have the highest strength. These are widely used for highly stressed structural components in aircraft as well as in a range of sporting goods, and so are readily available. Moreover, they have good machining properties. In common with previous workers (Paureau & Vettier, 1975), the 7075 Al alloy with a T6511 temper was selected for the pressure vessel under consideration here. The standard composition and approximate neutron attenuation length calculated from it are given in Table 2. 7075 T6 Al alloys typically have a 0.2% proof stress of about 500 MPa and an ultimate tensile strength of about 570 MPa. The bar of 7075 T6511 used here [89.60% Al, 5.40% Zn, 2.60% Mg, 1.60% Cu, 0.22% Cr, 0.58% others (weight %)] had a 0.2% proof stress of 577 MPa and an ultimate tensile strength of 637 MPa.

For a pressure vessel with internal diameter of 12 mm (allowing samples of up to 10 mm diameter) and a 5 mm wall thickness (giving a pressure-vessel wall thickness of 14.1 mm for a detected neutron to travel through, passing both into and out of the vessel at 45° to its axis), the ratio,  $K$ , of the external to internal diameter of the vessel is 1.83. For pressure vessels with  $K > 1.2$ , the HPTA safety code (High Pressure Technology Association, 1975) specifies that the yield pressure,  $p_y$ , of the vessel should be considered as given by

$$p_y = (\sigma_y/2)(1 - K^{-2}), \tag{1}$$

where  $\sigma_y$  is the 0.2% proof stress, and that the ultimate bursting pressure,  $p_b$ , of the vessel should be considered as given by

$$p_b = 2\sigma_u(K - 1)/(K + 1), \tag{2}$$

where  $\sigma_u$  is the ultimate tensile strength. The maximum working pressure should then not be greater than  $0.42p_b$  with pressure testing carried out to  $0.5p_b$ . Using  $\sigma_y = 577$  MPa,  $\sigma_u = 637$  MPa and  $K = 1.83$ , then  $p_y = 202$  MPa,  $p_b = 374$  MPa, and the maximum working pressure should be 157 MPa with pressure testing carried out to 187 MPa.

In order to check these guidelines, the circumferential and axial strains on the outer diameter of an exact replica of the pressure vessel were measured as a function of confining pressure at room temperature (294 K). In this experiment, the vessel was pressurized to 275 MPa, depressurized to 0 MPa, and then repressurized to 350 MPa. The axial and circumferential strains were measured by resistance strain gauges. Both strain circuits (axial and circumferential) were configured as a Wheatstone bridge containing two active strain gauges mounted about  $180^\circ$  apart on the outer diameter of the pressure vessel at about the position where the sample would be located, and two passive strain gauges mounted on a piece of the pressure material which was not deformed (Neubert, 1967). The results are shown in Fig. 2. From these it can be seen that during the first pressurization, the first sign of yielding (visible in the circumferential strain) occurred at about 185 MPa with significant yielding not occurring until a pressure of about 210 MPa. The depressurization of the vessel from 275 MPa and subsequent repressurization showed that it did not yield again until 275 MPa was attained, suggesting that there may be some benefit in overpressurizing the vessel

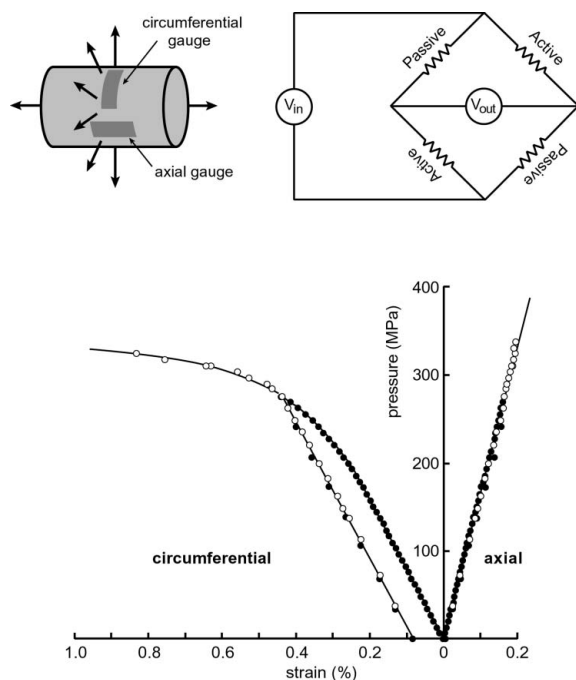


**Figure 2**

The results of pressure testing an exact replica of the pressure vessel. Top left: diagram showing the position and orientation of the active strain gauges. Two more active gauges were present on the hidden side of the vessel in this diagram. The arrows indicate schematically the loads produced by the confining pressure. Top right: the Wheatstone bridge configuration used for each strain-gauge circuit. Bottom: the circumferential and axial strains as a function of pressure. The results show initial yielding of the pressure vessel at about 185 MPa.

during pressure testing. Likewise, Blaschko & Ernst (1974) noted the advantages of autofrettaging in comparison with the more complex and expensive process of manufacturing a compound vessel when seeking an aluminium-alloy pressure vessel with superior strength properties. However, it should be noted that cold-working is not generally regarded as being very effective in improving the strength of 7000 series aluminium alloys. Nor are these alloys very ductile (elongation at failure is typically about 8%) and so overpressurizing them carries the risk of introducing permanent fatigue damage. The bursting tests carried out by Paureau & Vettier (1975) on autofrettaged 7075 T6 Al alloy cells with different wall ratios ( $1.7 < K < 3.0$ ) show that the actual bursting pressure is only underestimated by 5–10% by equation (2).

The HPTA safety code specifies for a vessel operating under creep conditions (*i.e.* where the creep stress at rupture after 100000 h,  $\sigma_{CR}$ , is greater than  $0.75\sigma_y$ ) that the maximum working pressure,  $p_{max}$ , should satisfy

$$p_{max} < (4/3)\sigma_{CR} [(K - 1)/(K + 1)]. \quad (3)$$

For  $K = 1.83$ , this requires  $p_{max} < 0.391\sigma_{CR}$ , which for a maximum working pressure of 160 MPa requires  $\sigma_{CR} > 409$  MPa.  $\sigma_{CR}$  at room temperature is not known, but at the nearest conditions for which the creep rupture properties of 7075 T6 Al alloy are known, *i.e.* at 348 K, the stress at creep rupture after 30000 h is 350 MPa. Hence at ambient conditions (293 K), we believe that this HPTA safety-code guideline is close to being satisfied. Likewise, the fatigue properties of the alloy are not well constrained, although the long-term fatigue endurance limit (the stress required to give a 50% probability of failure in rotary bending after 108 cycles) of 7075 T6 Al alloy is about 160 MPa. However, the HPTA safety code specifies that if all the safety requirements given above are satisfied, a vessel is extremely unlikely to fail in less than 1000 pressure cycles. The code specifies the following condition for an infinite vessel life,

$$p < [\sigma_u(K^2 - 1)/K^2]/8, \quad (4)$$

but with  $\sigma_u = 637$  MPa and  $K = 1.83$  this requires  $p < 56$  MPa. Rather than be restricted to such a low maximum working confining pressure, we have designed the pressure vessel to be easy to manufacture so that it can be frequently replaced. Given the limited ductility of the 7000 series aluminium alloys, this is a sensible precaution anyway when the vessel is used above 100 MPa.

#### 4. The pressure-vessel assembly

A diagram of the pressure-vessel assembly is shown in Fig. 3 as developed for a specimen of 6.3 mm diameter. This assembly comprises the vessel and sample assembly retaining pieces, the internal force gauge (discussed in §5), the sample assembly, the confining-pressure system, and adapters for connecting the vessel to the Instron load frame.

The vessel has an outer diameter of 25 mm, reduced to 22 mm adjacent to the sample position to decrease the thickness of material the neutrons must pass through. This

reduction in outer diameter is also convenient in establishing the position of the sample when the assembled apparatus is being centred in the neutron beamline. The vessel is threaded at both ends to take the assembly retaining pieces. These

prevent the sample assembly from being expelled when confining pressure is applied.

The sample assembly consists of cylindrical tool-steel rams, a thin aluminium sleeve and the moving ram seal. The aluminium sleeve is here used solely to align the sample assembly. For porous materials, it may also be used to keep the confining medium out of the sample if it is sealed using O-rings housed in the sleeve or the rams (*e.g.* Paterson *et al.*, 1982). The moving-ram seal is a nitrile O-ring with two brass 45° mitre rings (to prevent extrusion of the O-ring) and a steel sleeve, all held in place by retaining piece A. By lightly hand-tightening retaining piece A during assembly, the O-ring can be deformed to make the initial seal prior to pressurization. This type of seal (Paterson, 1962) has long been used successfully in triaxial rock-deformation apparatus up to several hundred MPa confining pressure. The pressure seal at the other end of the vessel is an O-ring seal of similar design, which is made against the force gauge.

Confining pressure is introduced *via* a 1 mm cross-bore at the force-gauge end of the assembly. The pressure fittings are retained by a steel collar around the vessel. The confining medium used is Fluorinert (3M, grade FC-77), which is a mixture of fluorinated hydrocarbons that does not freeze until much higher pressures than those that can conceivably be used with this pressure-vessel design. The confining pressure is applied using a 280 MPa hand pump. A pressure transducer and rupture disc are located in the pressure line. If necessary, a large-volume pressurized confining medium reservoir may also be located in line to prevent significant pressure increases during deformation as the specimen shortens and the free volume within the pressure vessel decreases.

The pressure-vessel assembly screws directly into the Instron load frame *via* adapters, one made as an integral part of retaining piece B which screws into the Instron load cell, and the other made as a separate piece which screws into the Instron crosshead.

In contrast to the room-pressure case, the design incorporates no device to measure the axial shortening of the sample. This must be determined (as is customary in fluid and gas confining-medium triaxial deformation apparatus) by calibrating the shortening of the axial column as a function of applied load at different pressures using a sample of known elastic stiffness. This calibration may then be used to subtract the shortening of the apparatus part of the axial column from the total shortening indicated by the crosshead position to give the shortening of sample at any applied load and confining pressure.

### 5. Internal force gauge

The axial load seen by any load cell located outside the pressure vessel includes not only the load applied to the sample, but also the load required to overcome friction between the O-ring and the ram at the moving ram seal. Since this frictional force is not small, it has become conventional practice for triaxial rock-deformation apparatus to incorporate an internal force gauge which records only the load

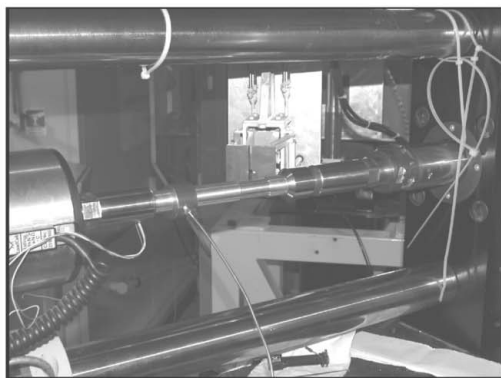
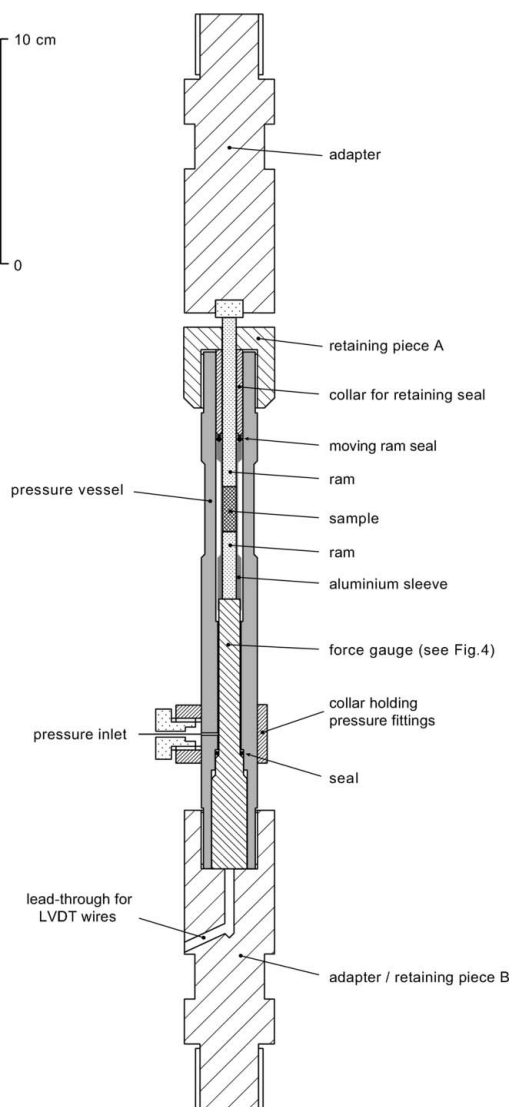


**Figure 3**  
Cross section of the pressure vessel, with a photograph of it in place on ENGIN-X.

applied to the sample. One of the most successful internal force gauges is based upon a design by H. C. Heard (here as modified by E. H. Rutter), in which the load is measured by the axial distortion of a hollow, but blind-ended, steel column (Fig. 4). A central unstressed rod is screwed into the blind-end and linked at the other end to the movable core of an a.c. linear variable differential transducer (LVDT). The LVDT itself is housed within the axial column and is pushed, by a spring, firmly up against a T-section tube which extends up the hollow column to a point a short way on the other side of the pressure seal. Consequently, when an axial load is applied and the hollow column shortens and displaces the unstressed rod out of the vessel relative to the LVDT, only that shortening between the top of the blind-ended central hole and the top of the T-section tube is measured. By calibrating this shortening as a function of load before inserting the force gauge into the pressure vessel, the load experienced by the sample may be determined during an experiment. Room-pressure calibration results for our force gauge are shown in Fig. 5.

There is a second-order sensitivity of the stiffness of the force gauge to confining pressure. Unfortunately, calibrating this pressure sensitivity requires measuring the output of the force gauge during loading at different confining pressures against an external load cell which also sees the seal friction. If

it can be assumed that the seal friction remains constant during loading, then the output of the force gauge can be calibrated against the difference between the load recorded on the load cell during loading and that recorded when loading first began. However, if this assumption were to be viable, then there would be no need for an internal force gauge. In practice, it is found that seal friction varies unpredictably during loading, especially if the axial strains are large and the ram travels a considerable distance through the seal area. To minimize these effects, we calibrated the force gauge against an external load cell at 160 MPa confining pressure using a sample of the same material as used for the rams. Since the deformation remained fully elastic, the travel of the ram through the seal area was small. The results of this calibration are shown in Fig. 5, where it can be seen that the pressure sensitivity of the force gauge is very small over the full working pressure range of the apparatus. As an example of the effect of varying friction during an experiment, in the experiment conducted at 160 MPa described below, where the axial strains were a few percent, the loads returned by the external load cell assuming constant friction were systematically 4% higher than those given by the force-gauge cali-

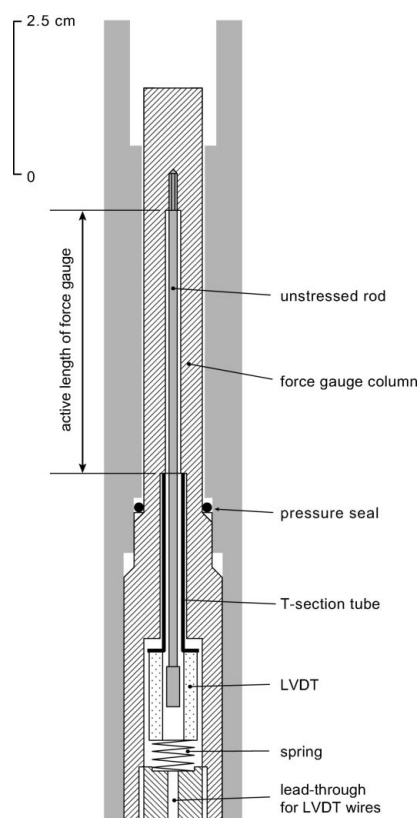


**Figure 4**  
Diagram of the internal force gauge. In the design shown, the important dimensions governing the sensitivity of the force gauge are the active length ( $43 \pm 0.5$  mm), and the outer and inner diameters of the hollow steel column over the active length (9.52 mm and 2.5 mm, respectively). The force gauge was made from AISI D2 tool steel, vacuum hardened and tempered to Rockwell C54.

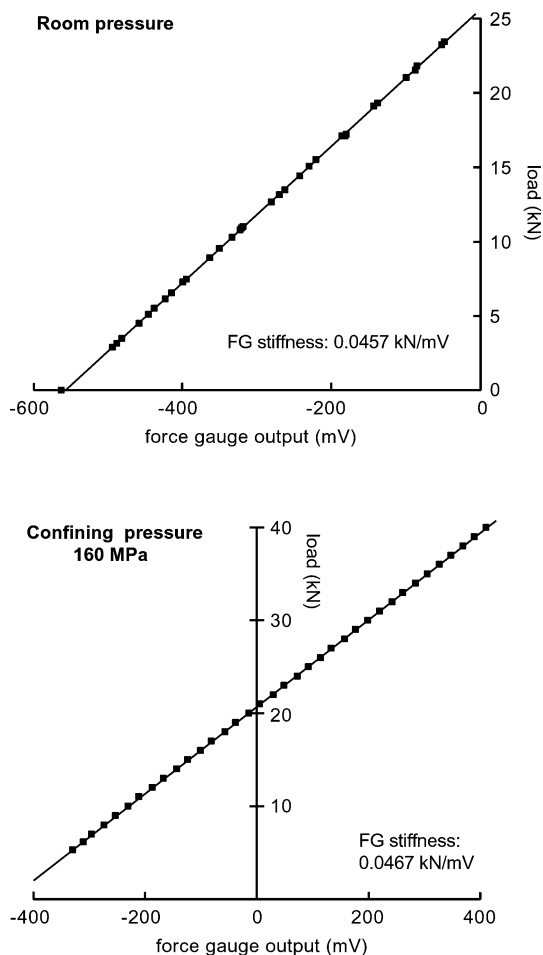


**Figure 5**  
Room-temperature (283 K) calibration data for the internal force gauge at room pressure (top) and at 160 MPa confining pressure (bottom).

bration, with the implication being that the friction steadily increased during deformation.

### 6. Commissioning experiments

The pressure-vessel apparatus was commissioned on ENGIN-X in a set of experiments designed to investigate the pressure sensitivity of the stress-induced austenite-to-martensite transformation in shape-memory NiTi alloy at room temperature (*e.g.* Vaidyanathan *et al.*, 1999). The results of these experiments will be described in detail elsewhere. Here attention is restricted to a comparison of the neutron diffraction patterns produced during deformation at room pressure without the pressure vessel present, with those produced during deformation at 160 MPa confining pressure using an identical experimental geometry but with the pressure vessel present.

The experiments were performed on cylindrical samples (~20 mm long by 6.29 mm diameter) which were cut from hot-rolled nitinol (55.8% Ni, 44.2% Ti) coil supplied by Special Metals Corporation, and then straightened and annealed.

The sample that was deformed at room pressure was loaded to 33 kN, initially in 5 kN steps (0 to 15 kN) and then subsequently in 1 kN steps (16 to 33 kN). The experimental geometry and procedure was as described above (§2). Diffraction patterns were collected at each load from a volume element of 7 × 4 × 4 mm located in the centre of the sample. The neutron count time was varied as follows: 30 μA (0 to 15 kN), 100 μA (16 to 22 kN) and 50 μA (23 to 33 kN), where ‘μA’ refers to the ISIS proton current, and results in counting periods at each load of approximately 10 min, 33 min and 17 min, respectively. A set of stacked diffraction patterns for part of the time-of-flight range that includes an austenite and a martensite peak are shown in Fig. 6. The transformation from austenite to martensite can be seen to begin at about 17 kN. Also apparent is the shift in peak positions with increasing load as both phases experience increasing elastic strain.

The sample that was deformed at 160 MPa confining pressure was taken to a differential load of 31.5 kN, initially in ~2 kN steps (0 to 12.3 kN) and subsequently in ~1 kN steps (13.3 to 31.5 kN). The neutron count time was fixed at 100 μA (approximately 35 min) for each load. The vessel operated leak-free for the full duration of the experiment (~16 h). A set of stacked diffraction patterns for the same part of the time-of-flight range as given for the room-pressure results are also shown in Fig. 6. The transformation from austenite to martensite can be seen to begin at about 15 kN. Again, the shift in peak positions with increasing load is visible. There is also a small peak from the pressure vessel. While not ideal, the presence of these peaks can be accommodated in a Rietveld-type data analysis by inclusion of the aluminium as an additional phase, particularly since the peak is weak and the pressure vessel does not deform (so that the peak position does not change). The signal-to-background ratio is comparable to that obtained after 50 μA at room pressure, indicating that the presence of the vessel and confining medium in the beamline requires an increase in count time of only about a

factor of two to produce neutron diffraction data of quality equivalent to that obtained from room-pressure experiments outside the pressure vessel.

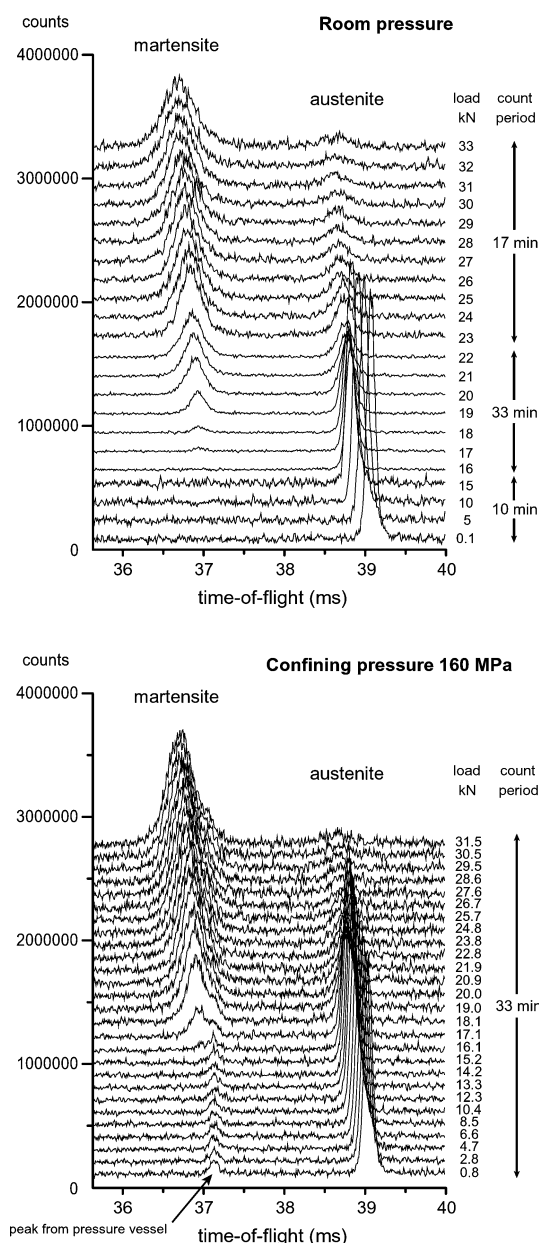


**Figure 6** Stacked neutron diffraction patterns over part of the time-of-flight range collected for NiTi samples deformed at room pressure (top) and at 160 MPa confining pressure (bottom). For the room-pressure data, each successive pattern (from low applied load to high) after the first is incremented by 150 000 counts parallel to the y axis, and for the 160 MPa confining-pressure data this increment is 100 000 counts. The room-pressure diffraction data were collected for three different counting periods (as indicated), but for presentational purposes, they have all been normalized to an equivalent incident neutron number (for a counting period of 50 μA, *i.e.* about 17 min); that is, the observed counts for the patterns generated at 0.1 to 15 kN have been multiplied by 1.67, and those observed at 18 to 22 kN have been divided by 2. In each case, the changing relative proportion of austenite and martensite phase is apparent in the changing peak intensities, while the increasing elastic strain in each phase is visible in the shift in peak position.

## 7. Summary and potential for design development

A simple aluminium-alloy pressure vessel suitable for use at room temperature has been developed which allows neutron diffraction data to be collected from cylindrical samples of up to 10 mm diameter, at confining pressures of up to 160 MPa, whilst they are also being deformed. The use of aluminium alloy as the pressure-vessel material means that these experiments cannot be conducted at more than slightly elevated temperatures. However, the commissioning results together with the use of aluminium-alloy pressure vessels in isostatic tests up to several hundred MPa suggest that there is considerable scope for increasing the vessel dimensions to permit larger samples and/or higher confining pressures. In the present design, increasing the vessel size will lead to an increase in the force applied to the load frame solely by the confining pressure (for the present vessel dimensions this is ~3 kN per 100 MPa). If this presents difficulties, then it is relatively straightforward to employ a pressure-balanced ram arrangement (*e.g.* Sammonds *et al.*, 1991). The design presented allows axial compression testing, but can be easily modified for axial extension and direct shear experiments (both under confining pressure) in the manner widely used in experimental rock-deformation research (*e.g.* Rutter *et al.*, 1985; Tullis & Tullis, 1986; Rutter, 1998).

## References

- Adams, B. L., Wright, S. I. & Kunze, K. (1993). *Metall. Trans. A*, **24**, 819–831.
- Birch, J. M., Wilshire, B., Owen, D. J. R. & Shantaram, D. (1976). *J. Mater. Sci.* **11**, 1817–1825.
- Blaschko, O. & Ernst, G. (1974). *Rev. Sci. Instrum.* **45**, 526–528.
- Carter, D. H. & Bourke, M. A. M. (2000). *Acta Mater.* **48**, 2885–2900.
- Covey-Crump, S. J., Schofield, P. F. & Stretton, I. C. (2001). *Geophys. Res. Lett.* **28**, 4647–4650.
- Cropper, D. R. & Pask, J. A. (1969). *Am. Ceram. Soc. Bull.* **48**, 555–558.
- Dann, J. A., Daymond, M. R., Edwards, L., James, J. A. & Santisteban, J. R. (2004). *Physica B*, **350**, E511–E514.
- Daymond, M. R., Bourke, M. A. M., Von Dreele, R. B., Clausen, B. & Lorentzen, T. (1997). *J. Appl. Phys.* **82**, 1554–1562.
- Daymond, M. R. & Priesmeyer, H. G. (2002). *Acta Mater.* **50**, 1613–1626.
- Dobson, D. P., Mecklenburgh, J., Alfe, D., Wood, I. G. & Daymond, M. R. (2005). *High Press. Res.* **25**, 107–118.
- Durham, W. B., Weidner, D. J., Karato, S.-I. & Wang, Y. (2002). *Plastic Deformation of Minerals and Rocks*, in *Review of Mineralogy and Geochemistry*, Vol. 51, edited by S.-I. Karato & H.-R. Wenk, pp. 21–49. Washington, DC: Mineralogical Society of America.
- High Pressure Technology Association (1975). *High Pressure Safety Code*. London: High Pressure Technology Association.
- Hutchings, M. T. & Windsor, C. G. (1987). *Neutron Scattering*, in *Methods of Experimental Physics*, Vol. 23C, edited by K. Sköld & D. L. Price, pp. 405–482. New York: Academic Press.
- Johnson, M. W. & Daymond, M. R. (2002). *J. Appl. Cryst.* **35**, 49–57.
- Lechner, R. (1966). *Rev. Sci. Instrum.* **37**, 1534–1537.
- Neubert, H. K. P. (1967). *Strain Gauges: Kinds and Uses*. London: Macmillan.
- Paterson, M. S. (1962). *J. Sci. Instrum.* **39**, 173–175.
- Paterson, M. S. (1990). *The Brittle–Ductile Transition in Rocks, The Heard Volume*, in *Geophysical Monographs*, Vol. 56, edited by A. G. Duba, W. B. Durham, J. W. Handin & H. F. Wang, pp. 187–194. Washington, DC: American Geophysical Union.
- Paterson, M. S., Chopra, P. N. & Horwood, G. R. (1982). *High Temp. High Press.* **14**, 315–318.
- Paureau, J. & Vettier, C. (1975). *Rev. Sci. Instrum.* **46**, 1484–1488.
- Prior, D. J., Boyle, A. P., Brenker, F., Cheadle, M. C., Day, A., Lopez, G., Peruzzo, L., Potts, G. J., Reddy, S., Spiess, R., Timms, N. E., Trimby, P., Wheeler, J. & Zetterström, L. (1999). *Am. Mineral.* **84**, 1741–1759.
- Rutter, E. H. (1998). *J. Struct. Geol.* **20**, 243–254.
- Rutter, E. H., Peach, C. J., White, S. H. & Johnston, D. (1985). *J. Struct. Geol.* **7**, 251–266.
- Sammonds, P. R., Murrell, S. A. F., Rist, M. A. & Butler, D. (1991). *Cold Reg. Sci. Technol.* **19**, 177–178.
- Schofield, P. F., Covey-Crump, S. J., Stretton, I. C., Daymond, M. R., Knight, K. S. & Holloway, R. F. (2003). *Mineral. Mag.* **67**, 967–987.
- Smith, F. A., Bradley, C. C. & Bacon, G. E. (1966). *J. Phys. Chem. Solids*, **27**, 925–930.
- Tullis, T. E. & Tullis, J. (1986). *Mineral and Rock Deformation: Laboratory Studies, The Paterson Volume*, in *Geophysical Monographs*, Vol. 36, edited by B. E. Hobbs & H. C. Heard, pp. 297–324. Washington, DC: American Geophysical Union.
- Vaidyanathan, R., Bourke, M. A. M. & Dunand, D. C. (1999). *J. Appl. Phys.* **86**, 3020–3029.
- Withers, P. J. (2004a). *J. Appl. Cryst.* **37**, 596–606.
- Withers, P. J. (2004b). *J. Appl. Cryst.* **37**, 607–612.